fractal and fractional

MDPI

Article

Fractional-Order Extremum Seeking Method for Maximum Torque per Ampere Control of Permanent Magnet Synchronous Motor

Haiying Song [1], Dejie Duan [1,*], Yiying Yan [1], Xinyao Li [1] and Min Xie [2]

[1] Department of Automatic Control, School of Automation, Guangdong Polytechnic Normal University, Guangzhou 510665, China; gsshy@gpnu.edu.cn (H.S.); 15089118518@163.com (Y.Y.); lixinyao@gpnu.edu.cn (X.L.)
[2] School of Electric Power, South China University of Technology, Guangzhou 510640, China; minxie@scut.edu.cn
* Correspondence: duandejie527@gmail.com

Abstract: Maximum torque per ampere (MTPA) control of internal permanent magnet synchronous motors (IPMSM) has become integral to high-efficiency motor drives. To minimize the influence of the traditional model-based analytical solution method on the MTPA control strategy due to the parameter variations during the motor operation, an online search MTPA method without model-based fractional-order extremum seeking control (FO-ESC) is proposed. Compared with the traditional integer-order ESC method, the Oustaloup approximation-based fractional-order calculus provides additional factors and possibilities for optimizing controller parameters to improve control performance. At the same time, the proposed approach does not require machine parameters and is thus not influenced by machine and drive nonlinearities. Simulation results show that the proposed method can ensure robust MTPA control under different loading conditions in real-time and improve the system's dynamic response speed and steady-state accuracy.

Keywords: maximum torque per ampere control; interior permanent magnet synchronous motor; extremum seeking algorithm; fractional-order calculus

Citation: Song, H.; Duan, D.; Yan, Y.; Li, X.; Xie, M. Fractional-Order Extremum Seeking Method for Maximum Torque per Ampere Control of Permanent Magnet Synchronous Motor. *Fractal Fract.* **2023**, *7*, 858. https://doi.org/10.3390/fractalfract7120858

Academic Editors: Allan G. Soriano-Sánchez and Didier López-Mancilla

Received: 24 October 2023
Revised: 27 November 2023
Accepted: 29 November 2023
Published: 30 November 2023

1. Introduction

Interior permanent magnet synchronous motors (IPMSMs) have a wide range of applications in the field of electric drives due to their high torque density, high efficiency, good mechanical characteristics, and wide range of constant power operation [1–3]. Compared with surface-mounted PMSMs (SPMSMs), due to the particular arrangement of permanent magnets in IPMSMs, their inductance convex polarity is significant, so in order to take full advantage of the reluctance torque generated by their convex polarity, IPMSMs usually do not impose a null *d*-axis current but instead use the maximum torque per ampere (MTPA) control [4]. At the same time, electric vehicles (EVs), at the forefront of the emerging new energy vehicle industry, are currently being widely promoted and adopted globally [5]. For the battery and motor, this control technique plays a vital role in the energy-efficient operation of EVs [6].

For IPMSM, due to the magnetic saturation of the rotor core, the cross-coupling between winding currents, and the uncertainty and nonlinearity of the machine parameters as well as the dependence of the parameters on temperature, the realization of accurate MTPA operation became one of the significant challenges facing the control technology of IPMSM. Therefore, many scholars have conducted a great deal of research on the MTPA control strategy of IPMSM [7,8]. The current MTPA control schemes can generally be divided into two categories: offline control strategies based on the mathematical model of the motor and online control strategies based on online search.

The most basic control strategy based on the mathematical model of the motor is the analytical solution approach [9], where the MTPA formula about the q- and d-axis currents is derived through theoretical and mathematical operations. However, these formulas depend on the motor parameters. In contrast, for real IPMSMs, the parameters vary according to the operating conditions, such as temperature, magnetic saturation, etc., resulting in bias in the MTPA strategy of the analytical solution method. In order to eliminate the deviation caused by parameter variations, the look-up tables (LUTs) method [10], the motor parameters calculation method [11], the maximum torque control (MTC) reference frame method [12], the scalar control (SC) method [13], etc., are used in MTPA control to obtain MTPA operating points through off-line experiments. However, such methods require prior knowledge of machine parameters such as stator resistance, inductance, etc., which requires much time for off-line experiments and cannot be directly applied to different motors due to different materials and manufacturing tolerances. In addition, one of the drawbacks of this method is the need for more robustness and the impossibility of off-line tracking any parameter variations or other differences between the mathematical model used for off-line computation and the actual electrodynamics.

One solution to overcome the poor robustness problem is to search online for MTPA operating conditions without relying on any pre-computed information or mathematical modeling of the machine. The on-line optimization strategy control of MTPA based on the principle of extremum seeking control (ESC) [14] can surmount the limitations of off-line MTPA control. ESC is an algorithm that adjusts the tracking MTPA operating point in a closed-loop manner without direct reference to the analysis of the motor model and related parameters and is highly adaptable to other motors. Currently, there are the following main types of realizations: high-frequency (HF) injection [15], low-frequency (LF) injection [16], virtual signal injection control (VSIC) [17], perturb and observe (P&O) technique [18], etc., the principles of which can be seen as an application of the ESC principle [19]. For instance, the work presented in [20] proposes an enhanced signal injection strategy responsible for correcting the MTPA reference deviation caused by motor parameter variations. It derives a parameter independent $-i_d/i_q$ with Te MTPA control law responsible for generating MTPA current references based on a constant parameter model to improve the dynamic performance of MTPA operation. Furthermore, a new virtual signal injection method was proposed in the literature [21], which compensates for the error caused by ignoring the higher-order bias terms in the traditional virtual signal injection strategy by fitting the q- and d-axis currents with higher order and superimposing them into the MTPA control law to obtain a more accurate MTPA operating point. An intriguing work in [22] was proposed, where a gradient descent-based algorithm is designed to introduce a small q-axis harmonic voltage into the machine to induce a small harmonic component in the motor speed. Velocity harmonic amplitude for MTPA angle detection is not dependent on the motor parameters and can reduce the error due to parameter variations. In literature [23], an ESC strategy was employed to determine the optimal reference flux in real-time based on the relationship between the stator magnetic chain and the stator current, resulting in an MTPA-like approach that improves the efficiency of direct torque control.

Fractional calculus is a 300-year-old topic extending the conventional integer-order calculus to any arbitrary order. The idea of fractional calculus has been known since the development of regular calculus, with the first reference probably being the letter between Leibniz and L'Hospital in 1695 [24]. But for a long time, it has been considered a singular mathematical problem. In recent years, since the introduction of fractional calculus into the field of engineering, the study of modeling physical phenomena using fractional-order calculus and fractional-order controllers has been widely conducted among researchers and scientists in the field [25,26]. There are some successful engineering applications reported in the literature for the PMSM control approach using fractional-order calculus. For example, the LUT-based fractional order composite controller was developed for the PMSM speed servo systems in [27]. The researcher represented the skin effect in a solid rotor by means of resistance and inductance with fixed values and fractional-order inductance, depending

on the frequency of induced eddy currents. Furthermore, to solve parameter fluctuations and disturbances, a novel fractional order model reference adaptive speed observer was proposed in [28] that estimates the rotor position and the angular velocity from the stator currents for sensorless control of PMSM. The authors of [29] have compared the design of a fractional-order proportional integral (FOPI) controller and an integer-order proportional integral controller for the PMSM speed regulation system, manipulating the current control scheme with a Xilinx FPGA chip to increase the system loop's bandwidth, and the accuracy of the numerical implementation of the fractional-order operator is investigated. In [30], a novel dead-time compensation method is introduced, which utilizes a FOPI controller to mitigate voltage errors. To address the dead-time effects, an enhanced particle swarm optimization algorithm is utilized for parameter design in the FOPI controller, resulting in accelerated convergence speed compared to other optimization algorithms.

With this motivation, the mathematical theoretical support of MTPA control is investigated, which is based on the traditional ESC strategy. An on-line search MTPA method based on fractional-order ESC (FO-ESC) is proposed. The fractional-order calculus in the extremum seeking optimization scheme is used to improve the convergence speed, robustness, and performance of the ESC method without increasing the complexity of the algorithm. A high-frequency sinusoidal excitation signal is superimposed on the stator current vector angle. A fractional-order filter is used to extract the gradient information of the current vector angle carried by the sinusoidal excitation signal. Then, a fractional-order integral optimizer determines the optimal current vector angle, thus realizing a more flexible and accurate MTPA control compared to existing work [31].

The remainder of this article is arranged as follows: Section 2 describes the mathematical model of IPMSM and the traditional model-based analytical solution method for the MTPA control strategy. Section 3 introduces the extremum seeking control algorithm and the regular ESC optimization theory. In Section 4, the mathematical model of FO-ESC under the Oustaloup algorithm is established. Section 5 illustrates the superiority and effectiveness of the proposed control method through simulation. Section 6 draws the conclusion of this article.

2. Permanent Magnet Synchronous Motor MTPA Control

2.1. Mathematical Modeling of IPMSM

When only the main factors influencing the motor are considered, the mathematical model of an IPMSM in the q- and d-axis reference frame can be expressed as follows:

$$\begin{cases} v_d = R_s i_d + L_d \frac{di_d}{dt} - p\omega_m L_q i_q, \\ v_q = R_s i_q + L_d \frac{di_q}{dt} + p\omega_m L_q i_d + p\omega_m L_q \psi_f. \end{cases} \tag{1}$$

The electromagnetic torque equation is:

$$Te = \frac{3}{2} p\psi_f i_q + \frac{3}{2} p(L_d - L_q) i_d i_q, \tag{2}$$

where i_q, i_d, v_q, v_d and L_q, L_d are the q- and d-axis currents, voltages, and inductances, respectively, R_s, ψ_f, p, ω_m and Te are the stator resistance, the mechanical permanent magnet flux linkage, the number of pole-pairs, the rotor angular speed, and the total electromagnetic torque, respectively.

2.2. MTPA Principle Analysis

In Equation (2), the first term is the permanent magnet component, and the second is the variable reluctance component. For SPMSM, the q- and d-axis inductance is almost equal, and the reluctance torque component can be neglected, so the null d-axis current control is an efficient control method for SPMSM. However, in IPMSM, the q-axis inductance is greater than the d-axis inductance, so if the null d-axis current control is still used, the

reluctance component cannot be fully utilized, so the q- and d-axis currents must be allocated reasonably, as shown in Figure 1. There are many combinations of the q- and d-axis currents to satisfy a specific load torque, such as points A and C. However, only point B is eligible for MTPA operating conditions, which satisfy both the following conditions:

$$\min |i_s| = \sqrt{i_d^2 + i_q^2}, \text{ subject to } Te = Te_0, \tag{3}$$

$$\begin{cases} i_d = i_s \cos \beta_{MTPA}, \\ i_q = i_s \sin \beta_{MTPA}, \end{cases} \tag{4}$$

where β_{MTPA} is the optimal current angle, Te_0 is the desired torque, $|i_s|$ is the magnitude of the stator current vector.

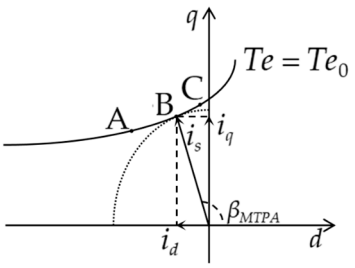

Figure 1. Stator current under a constant load torque.

By substituting Equation (4) into Equation (2), the torque can be rewritten as:

$$Te = \frac{3}{2} p \psi_f i_s \sin \beta + \frac{3}{4} p (L_d - L_q) i_s^2 \sin 2\beta. \tag{5}$$

From Equation (5), it can be seen that when Te is certain, there exists an optimal current angle β_{MTPA} between the stator current i_s and the current angle β, making the stator current amplitude $|i_s|$ to be minimized, and this current angle β_{MTPA} is the MTPA operating point.

The traditional mathematical model-based control strategy of the analytical solution method is derived from Equation (5) to obtain the optimal current angle:

$$\frac{\partial Te}{\partial \beta} = \frac{3}{2} p [\psi_f i_s \cos \beta_{MTPA} + (L_d - L_q) i_s^2 \cos 2\beta_{MTPA}] = 0. \tag{6}$$

Then, "β_{MTPA}" can be calculated using (6) for a given i_s:

$$\beta_{MTPA} = \arccos \left(\frac{-\psi_f + \sqrt{8(L_d - L_q)^2 i_s^2 + \psi_f^2}}{4(L_d - L_q) i_s} \right). \tag{7}$$

Substituting Equation (7) into Equation (4) yields the optimal MTPA reference current control combination. However, it is highly important to note from Equation (7) that the current angle depends on the motor parameters L_q, L_d, ψ_f, which vary nonlinearly according to the load conditions during machine operation [32], such as temperature, magnetic saturation, etc.; thus, it is challenging to achieve correct MTPA control with Equation (7).

Remark 1. *In this paper, a fractional-order extremum seeking control-based MTPA angle search algorithm is proposed, in which the stator current harmonic is used as the input signal and the MTPA angle is obtained if the current harmonic magnitude is minimized. The FO-ESC method does not require any machine parameters; thus, robust MTPA control can be achieved.*

3. Principles of Extremum Seeking Control

In order to reduce the error of the analytical solution method MTPA control due to the variation of motor parameters, an MTPA control strategy based on the principle of extremum seeking search is proposed. The extremum seeking search algorithm is a kind of adaptive control, while the model-independent real-time optimization method treats the model as a whole as a black box and achieves the optimality of the target output only through the feedback of certain states.

As shown in Equation (5), when the load torque is certain, i_s is an extreme value (minimum) function of β. The online MTPA strategy is to continuously search for and update this extreme value point when operating conditions change. More notably, Antonello, R. et al. provide a theoretical analysis of the MTPA control strategy based on the operating principle of extremum seeking control, which provides valuable insights into the system design procedure, investigates the convergence of the optimal operating point, and experimentally tests the strategy on an IPMSM [31].

The control block diagram of the traditional extremum seeking control is shown in Figure 2.

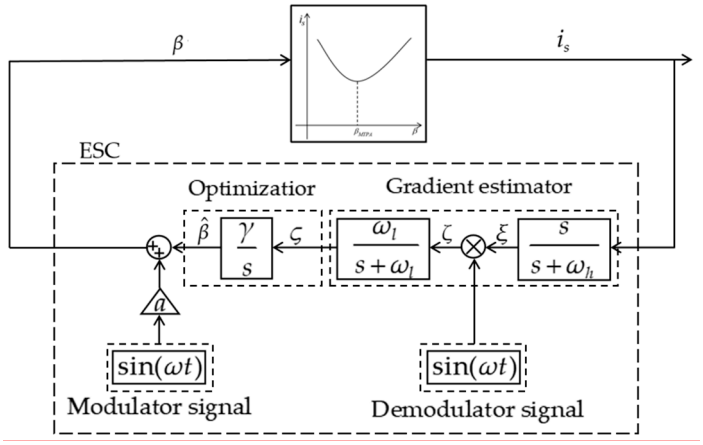

Figure 2. Schematic of the traditional extremum seeking control.

Where β is the input of the iterative search and γ is the coefficient of the optimization integrator, ω, a is the frequency and amplitude of the excitation signals, $\sin(\omega t)$ is the excitation signals (modulation and demodulation), i_s is the output of the objective function of the system to be optimized, ω_h, ω_l is the high-pass filter (HPF) and low-pass filter (LPF) cutoff frequencies of the gradient estimator.

According to Figure 2, the iterative steps of the ESC are summarized as follows:

In the first step, a small high-frequency modulation signal $a\sin(\omega t)$ is injected into the estimated current angle $\hat{\beta}$ of the motor stator current to obtain the phase angle of the motor stator current:

$$i_s^* = i_s(\hat{\beta} + a\sin(\omega t)). \tag{8}$$

Through the Taylor expansion, partial derivative terms above the second order are ignored because the value of the modulation signal amplitude a is very small and so it was sorted out:

$$i_s^* = i_s(\hat{\beta}) + \frac{\partial i_s}{\partial \hat{\beta}} a\sin(\omega t) + \frac{1}{2}\frac{\partial^2 i_s}{\partial \hat{\beta}^2}(a\sin(\omega t))^2 + \cdots = i_s(\hat{\beta}) + \frac{\partial i_s}{\partial \hat{\beta}} a\sin(\omega t). \tag{9}$$

In the second step, the DC term of i_s^* is filtered out by a HPF to obtain the following:

$$\xi = \frac{\partial i_s}{\partial \hat{\beta}} a\sin(\omega t). \tag{10}$$

In the third step, by multiplying ξ with $\sin(\omega t)$ to gets:

$$\zeta = \frac{\partial i_s}{\partial \hat{\beta}} a \sin^2(\omega t) = \frac{\partial i_s}{\partial \hat{\beta}} a(1 - \cos(2\omega t)). \tag{11}$$

In the fourth step, the LPF can be passed again to obtain information about the gradient between the stator current and the current angle:

$$\varsigma = a \frac{\partial i_s}{\partial \hat{\beta}}. \tag{12}$$

The fifth step, as shown in Figure 3, $\frac{\partial i_s}{\partial \hat{\beta}} = 0$ is satisfied only at the MTPA operating point β_{MTPA}, while $\frac{\partial i_s}{\partial \hat{\beta}} < 0$ is satisfied when $\beta < \beta_{MTPA}$ and $\frac{\partial i_s}{\partial \hat{\beta}} > 0$ is satisfied when $\beta > \beta_{MTPA}$. Thus, continuous excitation of current i_s constantly yields ς. Then, by integrating, the current angle β_{MTPA} for optimal MTPA operation can be updated in real-time.

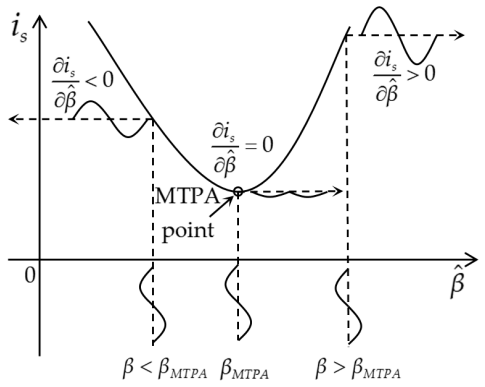

Figure 3. Stator current and vector angle MTPA tracking under a constant load torque.

4. Fractional-Order Extremum Seeking MTPA Strategy

The fractional-order extremum seeking algorithm is proposed in this work, in which fractional-order calculus operators are used in the extremum optimization process. Fractional-order calculus refers to fractional-order differentiation and integration, whose special form is integer-order calculus. The fractional-order model more realistically describes the behaviors of dynamic systems and takes into account non-local features [33], unlimited memory [34], etc. Compared to the traditional ESC, FO-ESC provides additional degrees of freedom with fractional-order factors, which provide more factors and possibilities for optimizing the controller parameters to fit the system characteristics and make the control system more flexible.

The fractional-order calculus operator is approximated using the Oustaloup algorithm in MATLAB and Simulink [35], which uses multiple integer-order filters to approximate the fractional-order calculus. When the fitted frequency is (ω_b, ω_g), the transfer function approximated by the Oustaloup method can be expressed as:

$$k(s) = \left(\frac{bs}{d\omega_b}\right)^{\alpha} \left(1 + \frac{-ds^2 + b}{ds^2 + b\omega_g s}\right)^{\alpha}, \tag{13}$$

where b and d are constant factors, Equation (13) can be rewritten by the first-order Taylor expansion:

$$k(s) \approx \left(\frac{bs}{d\omega_b}\right)^{\alpha} \left\{1 + \alpha \frac{-ds^2 + d}{ds^2 + b\omega_g s} + \frac{\alpha^2 - \alpha}{2} \left(\frac{-ds^2 + d}{ds^2 + b\omega_g s}\right)^2\right\}. \tag{14}$$

Thus, the fractional-order calculus operator s^{α} is expressed by:

$$s^{\alpha} = \left(\frac{d\omega_b}{b}\right)^{\alpha}\left(\frac{ds^2 + b\omega_g s}{d(1-\alpha)s^2 + b\omega_g s + d\alpha}\right)k(s). \tag{15}$$

More details regarding the Oustaloup algorithm can be found in [36,37].

Based on the introduction of the FO operator, fractional-order extremum seeking MTPA control can be achieved by using fractional-order filters in the gradient estimator and optimizer of the ESC, as in Figure 4, "s" will be replaced by "s^{α}" in gradient estimator and optimizer, where $0 < \alpha_1, \alpha_2, \alpha_3 < 1$, $\pi/2$ is the initial value of the current angle, κ is the excitation signal gain, and sgn(•) is:

$$\mathrm{sgn}(i_s) = \begin{cases} 1, & i_s \geq 0, \\ -1, & i_s < 0. \end{cases} \tag{16}$$

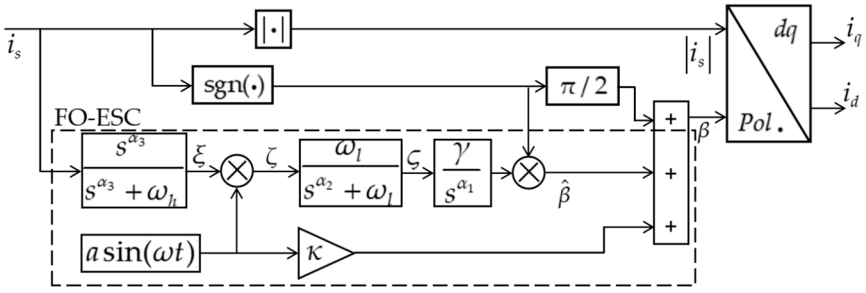

Figure 4. Detailed diagram of the proposed MTPA tracking controller.

The mathematical equations based on the FO-ESC method can be introduced according to Figure 4:

$$\begin{cases} i_s = i_s(\beta) + \frac{\partial i_s}{\partial \beta} \cdot a\sin(\omega t), \\ \beta = \kappa \cdot a\sin(\omega t) + \mathrm{sgn}(\bullet)\left[\frac{\pi}{2} + \frac{\gamma}{s^{\alpha_1}}\varsigma\right], \\ \varsigma = \frac{\omega_l}{s^{\alpha_2}+\omega_l} \cdot \zeta, \\ \zeta = a\sin(\omega t) \cdot \frac{s^{\alpha_3}}{s^{\alpha_3}+\omega_h} \cdot i_s. \end{cases} \tag{17}$$

Unlike previous improved ESC methods that use complex mathematical operations (e.g., Hessian matrix calculations) or additional feed-forward and feedback control loops, as shown in Equation (17), this method uses fractional-order calculus without increasing the complexity of the algorithm, which is capable of searching for the optimal operating current angle of the MTPA much faster and achieves faster convergence and higher robustness.

Based on the previous analysis, in order to obtain a better control performance of the FO-ESC, the parameter tuning includes frequency ω and amplitude a of the excitation signals, optimization integrator gain γ, the cutoff frequency of LPF ω_l and HPF ω_h, and fractional-order factors $\alpha_1, \alpha_2, \alpha_3$. The design procedure of the FO-ESC could be summarized as follows:

A. Select the excitation signal $a\sin(\omega t)$, and the optimization integrator gain γ:

The excitation signal frequency ω should be set as slow as possible compared to the plant. The large values of amplitude a and optimization integrator gain γ represent a larger range of extreme seeking and thus lead to faster convergence rates. However, the ESC sensitivity and oscillation amplitude are increased due to large values of a and γ. Thus, the selection of a and γ should consider the trade-off between system stability and convergence speed.

B. Design the HPF and LPF according to the frequency of the excitation signal:

Generally speaking, the HPF frequency ω_h should be slower than the excitation frequency ω, and the LPF frequency ω_l should be slower than the HPF frequency ω_h.

C. Fractional-order factors $\alpha_1, \alpha_2, \alpha_3$:

As mentioned before, the fractional-order factors $\alpha_1, \alpha_2, \alpha_3$ provide additional degrees of freedom with fractional-order factors for tuning the best controller performance.

In order to give an insight into the influences of fractional-order factors on the convergence performance of the FO-ESC and compare the performance of integer-order and FO-ESC numerically, these two algorithms are both applied to the double-integrator system [38]:

$$\begin{cases} \dot{x}_1 = x_2, \\ \dot{x}_2 = u, \end{cases} \tag{18}$$

with $u(t) = -30(x_1(t) - \delta(t)) - 11x_2(t)$ and the output $y(t) = -10(x_1(t) - 5)^2 + 10$. $y(t)$ reaches its maximum $y^* = 10$ at $x_1(t) = 5$. $x_1(0) = \delta(0) = 4$, $x_2(0) = 0$. The control system is explained in Figure 5, and the ESC and FO-ESC scheme are illustrated in Figures 2 and 4, respectively. The sensitivity analysis of $\alpha_1, \alpha_2, \alpha_3$ is shown in Figure 6.

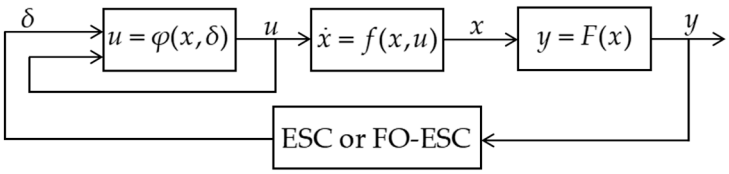

Figure 5. Double-integrator system with FO-ESC.

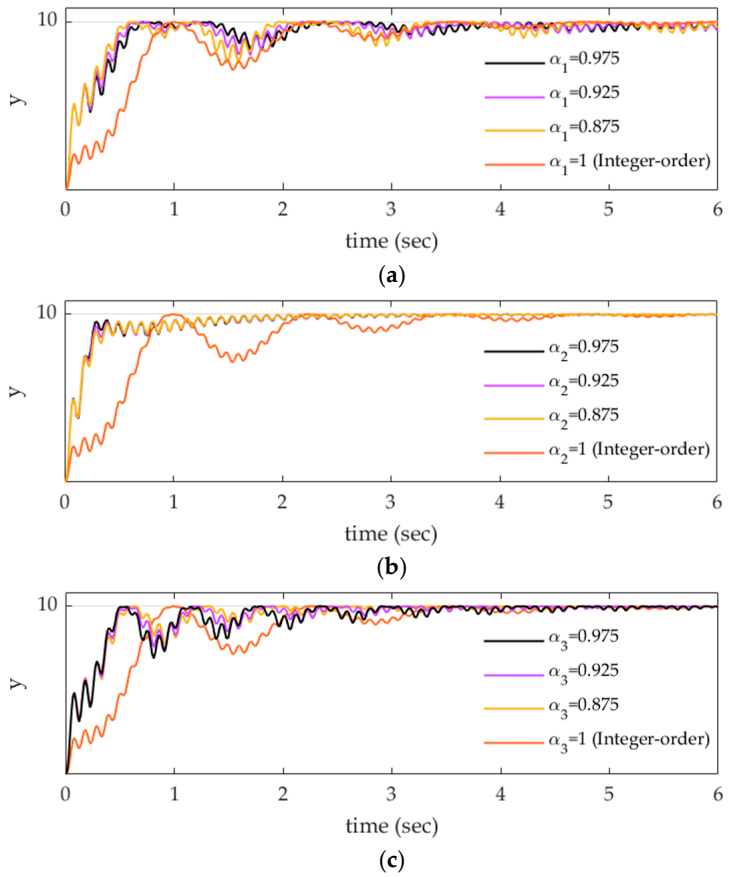

Figure 6. Sensitivity analyses of different fractional-order factors α. (**a**) differences in FO-ESC output when only the α_1 value is changed. (**b**) differences in FO-ESC output when only the α_2 value is changed. (**c**) differences in FO-ESC output when only the α_3 value is changed.

From the sensitivity analysis results, it can be seen that FO-ESC has faster tracking performance and higher accuracy than integer order. Therefore, the convergence speed of ESC is improved by using fractional order factors. In addition, it is observed that the fractional-order factor of LPF α_2 has the strongest influence on the convergence performance. This sensitivity analysis provides a handy guide for tuning the parameters of the fractional order factor in the ESC.

5. Simulation Verification

In order to verify the accuracy and speed of the MTPA control, the whole drive system has been simulated in the MATLAB/Simulink environment. The overall schematic of the IPMSM control system is based on the proposed control scheme, as shown in Figure 7. The q- and d-axis currents i_q, i_d are generated by the FO-ESC MTPA control law scheme illustrated in Figure 4.

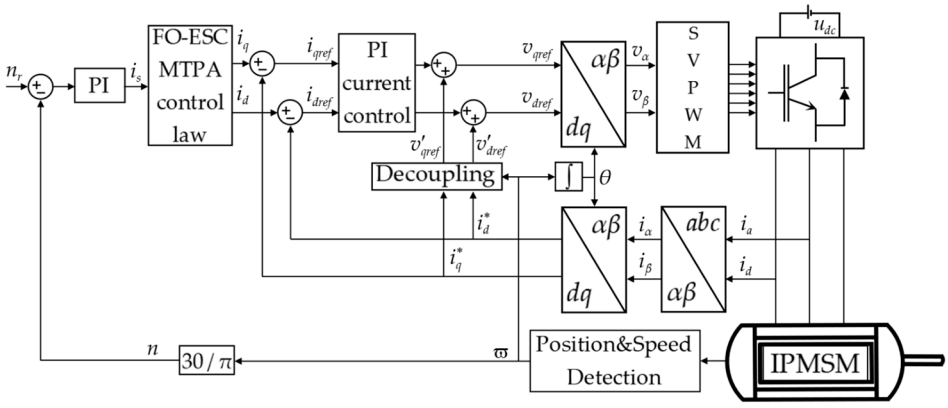

Figure 7. Overall schematic of the IPMSM drive control system.

The q- and d-axis currents will be compared with the measured q- and d-axis currents in PI current controllers to generate the reference q- and d-axis voltages after decoupling. The decoupling scheme illustrated in Figure 8.

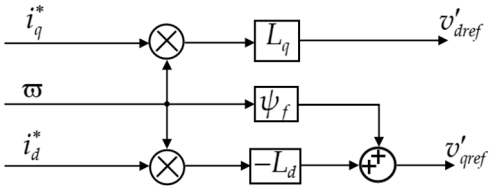

Figure 8. Schematic of the Decoupling block.

The motor specifications of the IPMSM and the proposed FO-ESC tracking controller parameters are given in Tables 1 and 2, respectively.

Table 1. Parameters of IPMSM.

Symbols	Parameters	Values
R	Phase resistance	0.077 Ω
p	Number of pole-pairs	4
J	Motor plus load Inertia	0.1 Kg·m^2
L_d	Nominal d-axis inductance	1.5 mH
L_q	Nominal q-axis inductance	3 mH
ψ_f	Nominal permanent magnet flux linkage	0.11 Wb

Table 2. MTPA controller parameters.

Symbols	Parameters	Values
κ	Gain	0.1
γ	Integrator coefficient	-0.1
a	Excitation amplitude	0.5 rad
ω	Excitation frequency	290π Hz
$\alpha_1, \alpha_2, \alpha_3$	Fractional coefficient	0.9
ω_h	HPF time constant	$1/10\pi$ s
ω_l	LPF time constant	$1/900\pi$ s

In IPMSM drives, the purpose of replacing conventional $i_d = 0$ strategy with the MTPA strategy is to reduce the current magnitude. Therefore, the current magnitude of the $i_d = 0$ method is compared with the traditional ESC and the proposed MTPA scheme at a speed of 200 r/min and a load torque of 20 N·m. For all the simulation results, the ESC is activated at 0.2 s and the FO-ESC is activated at 0.4 s. The current state based on different control methods results are shown in Figure 9a–c.

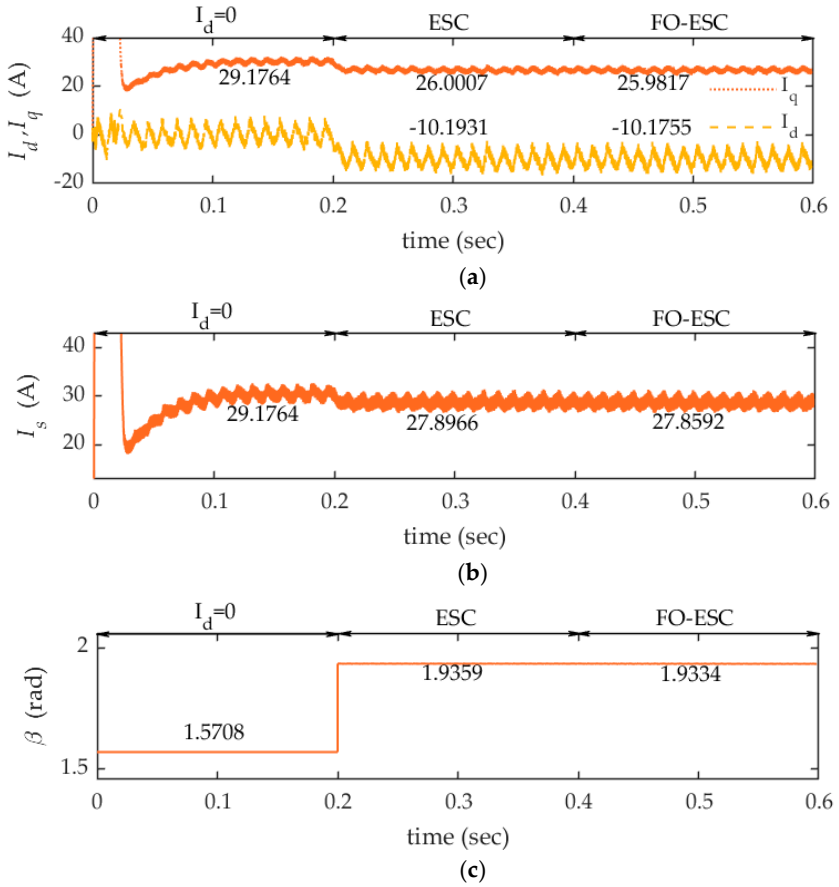

Figure 9. Comparison of different MTPA control strategies under a load torque of 20 N·m. (**a**) q- and d-axis current, (**b**) amplitude of the stator current, (**c**) current angle.

As shown in Figure 9a, the q-axis current reduced to 26.0007 A from 29.1874 A and d-axis current reduced to -10.1931 A from 0 A when the control algorithm was switched from the $i_d = 0$ method to the traditional ESC scheme; the q-axis current reduced to 25.9817 A from 26.0007 A and d-axis current reduced to -10.1755 A from -10.1931 A when the control algorithm was switched from the traditional ESC method to the FO-ESC scheme.

As shown in Figure 9b, the stator current magnitude was reduced accordingly to 27.8966 A from 29.1764 A when the control algorithm was switched from the $i_d = 0$ method

to the conventional ESC scheme and reduced to 27.8592 A from 27.8966 A when the control algorithm was switched from the traditional ESC method to the FO-ESC scheme.

As shown in Figure 9c, the current angle was increased accordingly to 1.9359 rad from 1.5708 rad when the control algorithm was switched from the $i_d = 0$ method to the traditional ESC scheme and to 1.9334 rad from 1.9359 rad when the control algorithm was switched from the conventional ESC method to the FO-ESC scheme.

In other words, the proposed MTPA scheme exhibits a lower current magnitude than the $i_d = 0$ method under the given load torque, verifies the effectiveness of the algorithm, and compares with the conventional ESC control without increasing the complexity of the algorithm. The FO-ESC control does not affect the accuracy of MTPA.

The transient response of the proposed MTPA scheme was simulated at 250 r/min under a step load torque of 15–25–15 N·m, and the simulation results of increasing and decreasing load torque are depicted in Figure 10a–c.

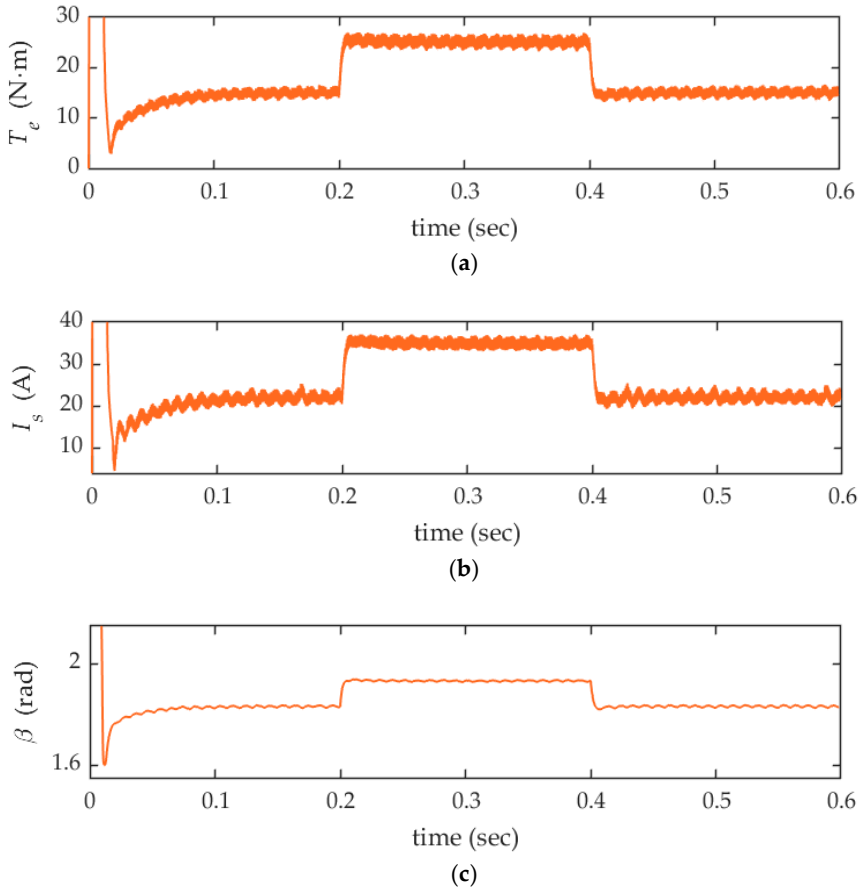

Figure 10. Transient response of the FO-ESC MTPA scheme at 250 r/min with a step load disturbance 15–25–15 N·m. (**a**) torque, (**b**) amplitude of the stator current, (**c**) current angle.

As shown in Figure 10a the load torque changed to 25 N·m from 15 N·m at 0.2 s and to 15 N·m from 25 N·m at 0.4 s. Figure 10b shows that the stator current magnitude was changed accordingly to 34.98 A from 22.27 A at 0.2 s and to 22.27 A from 34.98 A at 0.4 s. Figure 10c shows that the current angle changed to 1.97 rad from 1.82 rad at 0.2 s and to 1.82 rad from 1.97 rad at 0.4 s.

It can be observed that the motor is able to arrive at the new steady state within 0.003 s of the load sudden load addition and subtraction, which shows a fast MTPA tracking response.

The dynamic response of the proposed MTPA scheme was simulated at 10 N·m under a step reference speed of 50–150–100 r/min, and the simulation results of increasing and decreasing speed are depicted in Figure 11a–c.

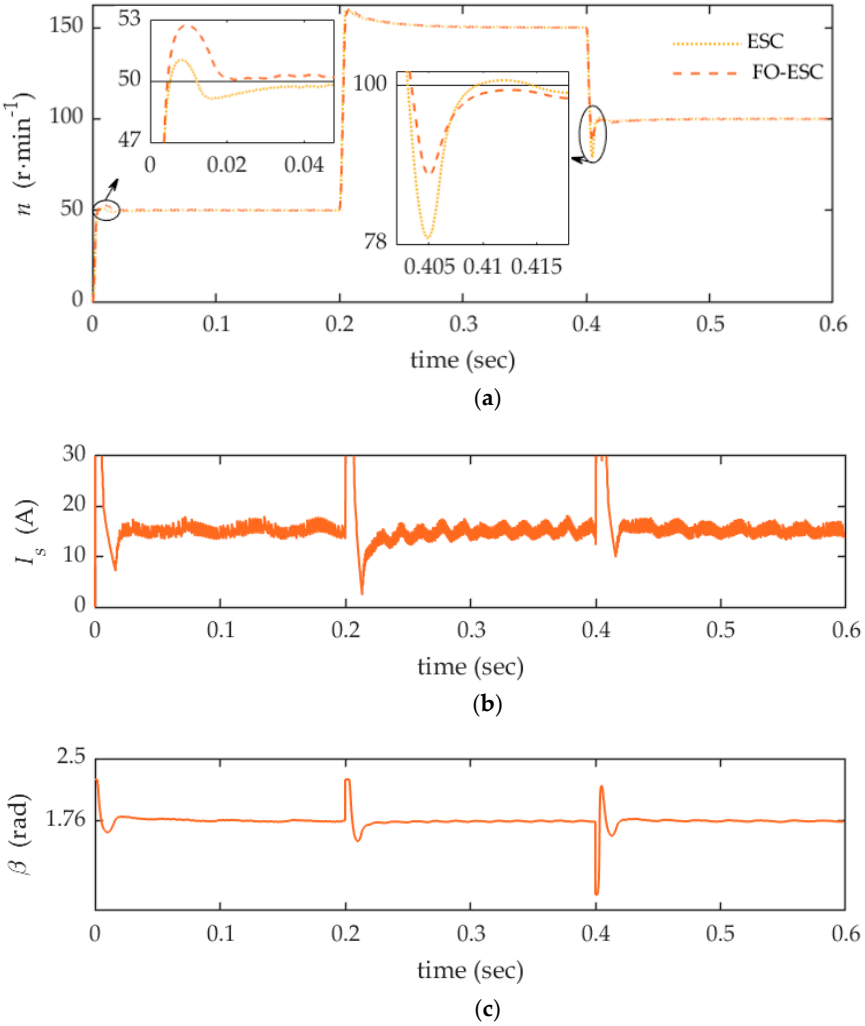

Figure 11. Dynamic response comparison between the traditional ESC and FO-ESC control strategies under different rotation speed. (**a**) speed, (**b**)amplitude of the stator current, (**c**) current angle.

In Figure 11a, the sudden speed change between the traditional ESC and FO-ESC control strategies under the same controller parameters was compared. When the speed command is run at 50 r/min, compared with the traditional ESC strategy, it is obvious to find that the FO-ESC control strategy reference speed changes from its initial value to the command speed at 0.02 s with fewer oscillations; for the speed command to suddenly increase or decrease, e.g., when it is reduced to 100 r/min from 150 r/min, the overshoot of the traditional ESC strategy is 22%. The overshoot of the FO-ESC strategy is 11%. Figure 11b,c show the stator's current magnitude and the angle's dynamic graphs. It can be seen that the change in speed under the command of load torque 10 N·m does not affect the magnitude of the stator current or current angle, which indicates the correctness of the control strategy. Thus, a comparison of the results shows that, under the same circumstances, the dynamic control effect is more flexible when the motor is suddenly accelerated or decelerated under FO-ESC control. It also shows that the proposed scheme can achieve a satisfactory dynamic response.

In addition, to further validate the robustness of motor parameter variations under the FO-ESC control strategy. By changing some parameters in the motor model. For example, L_q is changed to 2 mH from 3 mH and L_d is changed to 1 mH from 1.5 mH, the stator current variation of the proposed MTPA scheme was simulated at 300 r/min under a step load torque of 30–33–27 N·m, and the simulation results are depicted in Figure 12a,b.

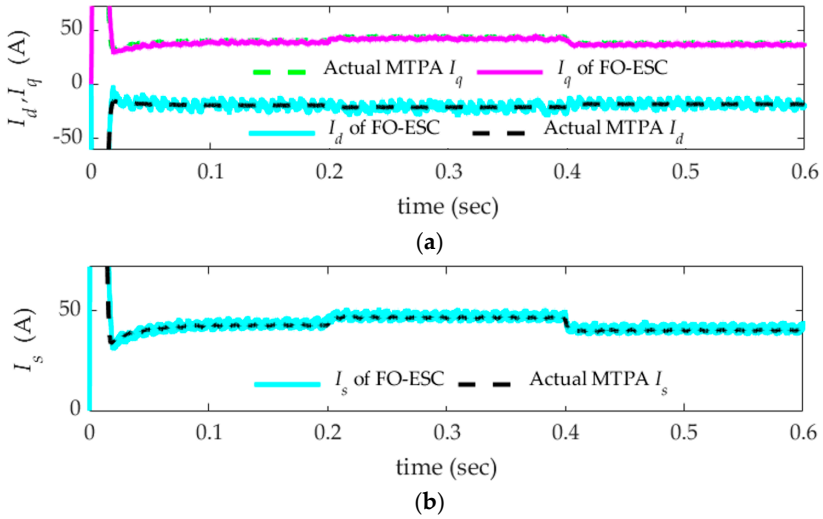

Figure 12. Dynamic response comparison between the traditional ESC and FO-ESC control strategies under different rotation speeds. (**a**) q- and d-axis current, (**b**) amplitude of the stator current.

Figure 12a,b shows the response of the motor stator current amplitude to a step change in torque. It can be seen that the current amplitude is initially large and then decreases rapidly until it reaches a minimum value for the MTPA condition. Moreover, when the load torque changed abruptly, the q- and d-axis currents were adjusted automatically until a new MTPA operation was reached. Therefore, it is verified that the scheme proposed in this paper can obtain a satisfactory dynamic response, and it is also shown that the control effect is not affected by the variation of motor parameters, which illustrates the robustness of the FO-ESC control scheme to torque disturbances.

In addition, based on the previous analysis, the algorithm execution time does not exceed 0.03 s. In other words, once the FO-ESC algorithm is enabled, the MTPA operation reaches its optimum within 0.03 s.

6. Conclusions

Aiming at the problem that the MTPA control strategy is based on the motor's mathematical model, it is impossible to off-line track any parameter variations or other differences between the mathematical model used for off-line computation and the actual electrodynamics. A fractional-order extremum seeking control (FO-ESC) online MTPA method that is not model-based is proposed. In this work, we have studied and analyzed the traditional extremum seeking algorithm maximum torque-current ratio control strategy and proposed a new fractional-order extremum seeking algorithm control. Compared with the traditional extremum seeking algorithm, by introducing the fractional-order differential integral operator, the degree of freedom of the control strategy is improved without increasing the algorithm's complexity, which makes its control of the system more flexible. The simulation results verify the control accuracy of the fractional-order extremum seeking MTPA strategy, the correct validity of the MTPA angle search under different speeds and load conditions, and the good dynamic and static tracking performance and flexibility of the strategy, which achieves the expected results.

The simulation results demonstrate that the proposed MTPA scheme has a faster convergence speed and a smoother tracking response without prior knowledge of motor parameters and is robust concerning torque and parameter variations. However, the MTPA control can only minimize the copper loss of the machine, which is a typical current control strategy below the base speed (i.e., in the constant-torque region), so this study focuses on the region below the base speed. Iron losses will increase significantly when the machine operates above the base speed (i.e., in the constant-power region). In this case, maximum efficiency control will be more appropriate for reducing motor loss. Investigations on

extending the proposed approach to maximum efficiency control will be conducted in our future work.

Author Contributions: Conceptualization, H.S. and D.D.; data curation, H.S.; formal analysis, D.D. and X.L.; funding acquisition, H.S. and M.X.; investigation, D.D.; methodology, H.S.; project administration, H.S.; resources, H.S.; software, D.D.; supervision, H.S.; validation, H.S. and D.D.; visualization, Y.Y.; writing–original draft, D.D.; writing–review and editing, H.S., X.L. and M.X. All authors have read and agreed to the published version of the manuscript.

Funding: This work was supported by the Guangdong Provincial Natural Science Foundation of China [2021A1515012245] and the Guangdong Basic and Applied Basic Research Foundation [2022A1515240074]. the Guangzhou Science and Technology Plan Project of the People's Livelihood Project [202002020052].

Data Availability Statement: The data presented in this study are not available due to privacy.

Conflicts of Interest: The authors declare no conflict of interest.

References

1. Zheng, S.; Zhu, X.; Xiang, Z.; Xu, L.; Zhang, L.; Lee, C.H. Technology trends, challenges, and opportunities of reduced-rare-earth PM motor for modern electric vehicles. *Green Energy Intell. Transp.* **2022**, *1*, 100012. [CrossRef]
2. Shi, T.; Yan, Y.; Zhou, Z.; Xiao, M.; Xia, C. Linear quadratic regulator control for PMSM drive systems using nonlinear disturbance observer. *IEEE Trans. Power Electron.* **2019**, *35*, 5093–5101. [CrossRef]
3. Seo, D.W.; Bak, Y.; Lee, K.B. An improved rotating restart method for a sensorless permanent magnet synchronous motor drive system using repetitive zero voltage vectors. *IEEE Trans. Ind. Electron.* **2019**, *67*, 3496–3504. [CrossRef]
4. Dai, C.; Guo, T.; Yang, J.; Li, S. A disturbance observer-based current-constrained controller for speed regulation of PMSM systems subject to unmatched disturbances. *IEEE Trans. Ind. Electron.* **2020**, *68*, 767–775. [CrossRef]
5. He, H.; Sun, F.; Wang, Z.; Lin, C.; Zhang, C.; Xiong, R.; Zhai, L. China's battery electric vehicles lead the world: Achievements in technology system architecture and technological breakthroughs. *Green Energy Intell. Transp.* **2022**, *1*, 100020. [CrossRef]
6. Heidari, H.; Rassõlkin, A.; Kallaste, A.; Vaimann, T.; Andriushchenko, E.; Belahcen, A.; Lukichev, D.V. A review of synchronous reluctance motor-drive advancements. *Sustainability* **2021**, *13*, 729. [CrossRef]
7. Li, Z.; O'Donnell, D.; Li, W.; Song, P.; Balamurali, A.; Kar, N.C. A comprehensive review of state-of-the-art maximum torque per ampere strategies for permanent magnet synchronous motors. In Proceedings of the 2020 10th International Electric Drives Production Conference (EDPC), Ludwigsburg, Germany, 8–9 December 2020; IEEE: Piscataway, NJ, USA; pp. 1–8.
8. Tinazzi, F.; Bolognani, S.; Calligaro, S.; Kumar, P.; Petrella, R.; Zigliotto, M. Classification and review of MTPA algorithms for synchronous reluctance and interior permanent magnet motor drives. In Proceedings of the 2019 21st European Conference on Power Electronics and Applications (EPE'19 ECCE Europe), Genova, Italy, 3–5 September 2019; IEEE: Piscataway, NJ, USA; p. P-1.
9. Uddin, M.N.; Radwan, T.S.; Rahman, M.A. Performance of interior permanent magnet motor drive over wide speed range. *IEEE Trans. Energy Convers.* **2002**, *17*, 79–84. [CrossRef]
10. de Kock, H.W.; Rix, A.J.; Kamper, M.J. Optimal torque control of synchronous machines based on finite-element analysis. *IEEE Trans. Ind. Electron.* **2009**, *57*, 413–419. [CrossRef]
11. Huang, W.; Zhang, Y.; Zhang, X.; Sun, G. Accurate torque control of interior permanent magnet synchronous machine. *IEEE Trans. Energy Convers.* **2013**, *29*, 29–37. [CrossRef]
12. Hida, H.; Tomigashi, Y.; Kishimoto, K. Novel sensorless control for pm synchronous motors based on maximum torque control frame. In Proceedings of the 2007 European Conference on Power Electronics and Applications, Aalborg, Denmark, 2–5 September 2007; IEEE: Piscataway, NJ, USA; pp. 1–10.
13. Consoli, A.; Scelba, G.; Scarcella, G.; Cacciato, M. An effective energy-saving scalar control for industrial IPMSM drives. *IEEE Trans. Ind. Electron.* **2012**, *60*, 3658–3669. [CrossRef]
14. Tan, Y.; Moase, W.H.; Manzie, C.; Nešić, D.; Mareels, I.M. Extremum seeking from 1922 to 2010. In Proceedings of the 29th Chinese Control Conference, Beijing, China, 29–31 July 2010; IEEE: Piscataway, NJ, USA; pp. 14–26.
15. Bolognani, S.; Sgarbossa, L.; Zordan, M. Self-tuning of MTPA current vector generation scheme in IPM synchronous motor drives. In Proceedings of the 2007 European Conference on Power Electronics and Applications, Aalborg, Denmark, 2–5 September 2007; IEEE: Piscataway, NJ, USA; pp. 1–10.
16. Antonello, R.; Carraro, M.; Zigliotto, M. Theory and implementation of a MTPA tracking controller for anisotropic PM motor drives. In Proceedings of the IECON 2012-38th Annual Conference on IEEE Industrial Electronics Society, Montreal, QC, Canada, 25–28 October 2012; IEEE: Piscataway, NJ, USA; pp. 2061–2066.
17. Sun, T.; Long, L.; Yang, R.; Li, K.; Liang, J. Extended virtual signal injection control for MTPA operation of IPMSM drives with online derivative term estimation. *IEEE Trans. Power Electron.* **2021**, *36*, 10602–10611. [CrossRef]

18. Windisch, T.; Hofmann, W. A comparison of a signal-injection method and a discrete-search algorithm for MTPA tracking control of an IPM machine. In Proceedings of the 2015 17th European Conference on Power Electronics and Applications (EPE'15 ECCE-Europe), Montreal, QC, Canada, 25–28 October 2012; IEEE: Piscataway, NJ, USA; pp. 1–10.
19. Zhang, C.; Ordóñez, R. *Extremum-Seeking Control and Applications: A Numerical Optimization-Based Approach*; Springer Science & Business Media: Berlin, Germany, 2011.
20. Li, K.; Wang, Y. Maximum torque per ampere (MTPA) control for IPMSM drives using signal injection and an MTPA control law. *IEEE Trans. Ind. Inform.* **2019**, *15*, 5588–5598. [CrossRef]
21. Sun, T.; Koç, M.; Wang, J. MTPA control of IPMSM drives based on virtual signal injection considering machine parameter variations. *IEEE Trans. Ind. Electron.* **2017**, *65*, 6089–6098. [CrossRef]
22. Lai, C.; Feng, G.; Mukherjee, K.; Tjong, J.; Kar, N.C. Maximum torque per ampere control for IPMSM using gradient descent algorithm based on measured speed harmonics. *IEEE Trans. Ind. Inform.* **2017**, *14*, 1424–1435. [CrossRef]
23. Mahmud, M.H.; Wu, Y.; Zhao, Y. Extremum seeking-based optimum reference flux searching for direct torque control of interior permanent magnet synchronous motors. *IEEE Trans. Transp. Electrif.* **2019**, *6*, 41–51. [CrossRef]
24. Monje, C.A.; Chen, Y.; Vinagre, B.M.; Xue, D.; Feliu-Batlle, V. *Fractional-Order Systems and Controls: Fundamentals and Applications*; Springer Science & Business Media: Berlin, Germany, 2010.
25. Zhou, D.; Zhang, K.; Ravey, A.; Gao, F.; Miraoui, A. Parameter sensitivity analysis for fractional-order modeling of lithium-ion batteries. *Energies* **2016**, *9*, 123. [CrossRef]
26. Petras, I. Stability of fractional-order systems with rational orders. *arXiv* **2008**, arXiv:0811.4102.
27. Zheng, W.; Huang, R.; Luo, Y.; Chen, Y.; Wang, X.; Chen, Y. A look-up table based fractional order composite controller synthesis method for the pmsm speed servo system. *Fractal Fract.* **2022**, *6*, 47. [CrossRef]
28. Niu, H.; Liu, L.; Jin, D.; Liu, S. High-Tracking-Precision Sensorless Control of PMSM System Based on Fractional Order Model Reference Adaptation. *Fractal Fract.* **2022**, *7*, 21. [CrossRef]
29. Wang, B.; Wang, S.; Peng, Y.; Pi, Y.; Luo, Y. Design and high-order precision numerical implementation of fractional-order PI controller for PMSM speed system based on FPGA. *Fractal Fract.* **2022**, *6*, 218. [CrossRef]
30. Li, F.; Luo, Y.; Luo, X.; Chen, P.; Chen, Y. Optimal FOPI Error Voltage Control Dead-Time Compensation for PMSM Servo System. *Fractal Fract.* **2023**, *7*, 274. [CrossRef]
31. Antonello, R.; Carraro, M.; Zigliotto, M. Maximum-torque-per-ampere operation of anisotropic synchronous permanent-magnet motors based on extremum seeking control. *IEEE Trans. Ind. Electron.* **2013**, *61*, 5086–5093. [CrossRef]
32. Liu, Z.H.; Li, X.H.; Wu, L.H.; Zhou, S.W.; Liu, K. GPU-accelerated parallel coevolutionary algorithm for parameters identification and temperature monitoring in permanent magnet synchronous machines. *IEEE Trans. Ind. Inform.* **2015**, *11*, 1220–1230. [CrossRef]
33. Malek, H.; Chen, Y. Fractional order extremum seeking control: Performance and stability analysis. *IEEE/ASME Trans. Mechatron.* **2016**, *21*, 1620–1628. [CrossRef]
34. Tang, Y.; Zhang, X.; Zhang, D.; Zhao, G.; Guan, X. Fractional order sliding mode controller design for antilock braking systems. *Neurocomputing* **2013**, *111*, 122–130. [CrossRef]
35. Trigeassou, J.C.; Maamri, N.; Sabatier, J.; Oustaloup, A. State variables and transients of fractional order differential systems. *Comput. Math. Appl.* **2012**, *64*, 3117–3140. [CrossRef]
36. Zhou, D.; Al-Durra, A.; Matraji, I.; Ravey, A.; Gao, F. Online energy management strategy of fuel cell hybrid electric vehicles: A fractional-order extremum seeking method. *IEEE Trans. Ind. Electron.* **2018**, *65*, 6787–6799. [CrossRef]
37. Yu, W.; Luo, Y.; Pi, Y. Fractional order modeling and control for permanent magnet synchronous motor velocity servo system. *Mechatronics* **2013**, *23*, 813–820. [CrossRef]
38. Yin, C.; Chen, Y.; Zhong, S.M. Fractional-order sliding mode based extremum seeking control of a class of nonlinear systems. *Automatica* **2014**, *50*, 3173–3181. [CrossRef]